Journal of Nanostructure in Chemistry (2020) 10:9–18
https://doi.org/10.1007/s40097-019-00324-x

ORIGINAL RESEARCH

Reduced graphene oxide-intercalated graphene oxide nano-hybrid for enhanced photoelectrochemical water reduction

Belete Asefa Aragaw[1]

Received: 7 September 2019 / Accepted: 7 December 2019 / Published online: 12 December 2019

Abstract

This paper reports on the synthesis of reduced graphene oxide (RGO)-intercataled graphene oxide (GO) nano-hybrid and investigates its application in photoelectrochemical (PEC) water reduction. The optical, structural, and morphological properties of RGO-intercalated GO (RGO/GO) nano-hybrid were studied using UV–Visible spectroscopy, X-ray diffraction, and scanning electron microscopy, respectively. The reduction of GO to RGO was studied using FTIR spectroscopy. The XRD and FTIR investigation shows the strong π–π stacking interactions between the layered GO host–RGO guest sheets. An improvement in PEC water reduction activity was exhibited by RGO/GO nano-hybrid photoelectrode, with a maximum photocurrent of − 61.35 μA/cm^2 for RGO 1 wt% in GO versus − 42.80 μA/cm^2 for pristine GO photoelectrode (43% improvement). The mechanism for photocurrent enhancement was studied by electrochemical impedance analysis. The PEC performance enhancement of RGO/RO nano-hybrid photoelectrode is attributed to the strong π–π stacking interactions between RGO and GO, leading to superior electron collection and transportation by RGO and hence reduced charge carrier recombination. In addition, the UV–Visible absorption and Taut plot analysis showed the higher light harvesting efficiency of the RGO/GO compared to GO, displaying a band gap of 2.58 eV and 3.11 eV for RGO/GO and GO, respectively. The findings of this work show the potential of a strongly coupled layered host–guest nano-hybrids for high-performance optoelectronic materials.

Graphic abstract

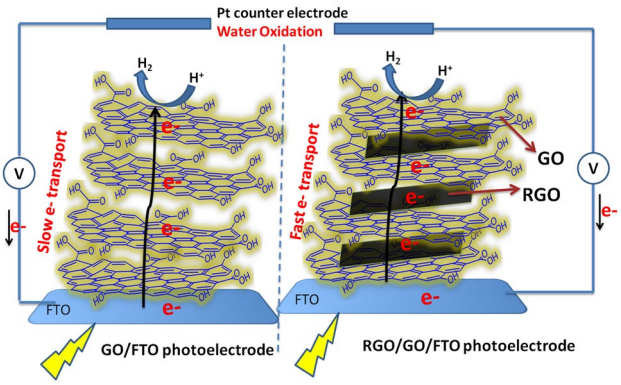

Keywords Graphene oxide · Reduced graphene oxide · Nano-hybrid · Photoelectrode · Water reduction · Photoelectrochemical cell

Introduction

The rise in demand for sustainable and carbon-free energy production drives the advancement of solar to electrical energy conversion and solar to chemical energy storage

✉ Belete Asefa Aragaw
beliyeeed@gmail.com

[1] Department of Chemistry, Bahir Dar University, P.O. Box 79, Bahir Dar, Ethiopia

systems. Solar energy storage in hydrogen fuel generated through photoelectrochemical (PEC) water reduction, known since the first report by Fujishima and Honda [1], is a promising way to address energy and environmental issues. The realization of such energy storage technologies is limited by solar to hydrogen fuel conversion efficiency of the system, which mainly depends on the property of the material that captures light energy and also design and architecture of the device. Several metal oxide semiconductor materials, such as TiO_2 [2], Fe_2O_3 [3], CuO [4, 5], and WO_3 [6] have been studied for PEC H_2 fuel production from water. However, only few non-metallic oxide semiconductor materials are available for this purpose. The most common are graphitic carbon nitride and graphene oxide. Graphene oxide (GO) is a polyaromatic two-dimensional carbon sheet produced by the exfoliation of natural graphite flakes. The advantages of GO include its non toxicity, low cost of the precursor material, and easy synthesis. In addition, the lager surface area of GO relative to other inorganic metal oxide and chalcogenide semiconducting materials [7]—one of the precondition for maximal adsorption of water molecule on the catalyst surface—caught researchers' attention as a promising photocatalytic material [8, 9]. Moreover, the hydrophilic nature and electrical properties of GO can be tuned by controlling the amount of oxygen containing functional groups introduced during oxidation of graphite. Due to the aforementioned advantages, GO is investigated for various purposes including photocatalytic and photoelectrochemical hydrogen fuel production from water [1, 9–16], photocatalytic decomposition of organic pollutants [17, 18], photocatalytic CO_2 to methanol and formic acid conversion [19–23], photocatalytic disinfection and water purification [24–26]. However, pristine GO has some limitations in photoelectrochemical energy conversion efficiency due to its lower electrical conductivity and higher photoelectron–hole charge carrier recombination. Several strategies have been proposed to alleviate these problems and enhance the photoelectrochemical hydrogen production efficiency. These are doping and coupling of GO with other materials [27–29]. The best candidate materials for this purpose are one of the GO's families, i.e., reduced graphene oxide (RGO). It is the reduced form of GO, where removing the oxygen containing functionalities and restoring the C=C double bond conjugation (aromaticity) give better electrical conducting property. RGO has been used in several investigations to enhance the electrical conductivity of semiconductor materials. For example, graphene has been used to improve the efficiency of solar hydrogen production with photoelectrode made from Cu_2O [5], Fe_2O_3 [30], $BiVO_4$ [27], TiO_2 [31], and graphitic C_3N_4 [32–34]. However, to the best of our knowledge, there is no research report on the use of RGO-coupled GO to improve the limitations of pristine GO. Here, the paper reports on the synthesis of RGO-coupled GO to fabricate RGO/GO nano-hybrid photoelectrode and investigates its application in PEC water reduction.

In this study, RGO/GO nanocomposite was synthesized by impregnating solutions of RGO and GO followed by drop-casting the RGO/GO solution on FTO glass to make FTO/RGO/GO photoelectrode and investigated its photoelectrochemical activity towards water reduction. The PEC activity improvement could be due to special π–π stacking interaction between the 2-dimensional structured RGO and GO. A strong π–π stacking interaction would be created between the e-rich RGO and e-deficient GO which leads to good photoelectron flow from GO to RGO according to Sanders and Hunters model [35]. Additional mode of interaction includes H-bonding due to the presence of O-containing functional groups. This strong interaction between the RGO and GO sheets forms a strongly coupled RGO/GO nanocomposite improving the electron transfer rate and lowering charge carrier recombination, thereby enhancing the PEC performance of RGO/GO nanocomposite relative to GO.

Experimental

Materials and preparation

The preparation of graphene oxide was based on the method reported by Hummer [36]. Ice-cooled concentrated H_2SO_4 (138 ml), graphite powder (3 g) and $NaNO_3$ (3 g) were mixed well by stirring. $KMnO_4$ (9 g) was added slowly under stirred and cooled condition. The mixture was removed from ice bath and stirred for 40 min. at 35 °C. Slow addition of water was performed which raised the temperature to 98 °C. Finally, 280 ml of deionized water and 18 ml of H_2O_2 (30%) was added consecutively to end the reaction. The graphene oxide prepared was treated with 5% HCl to neutralize the pH. RGO was prepared by reducing graphene oxide (1 mg/ml) using 4-ml hydrazine at 80 °C for 24 h. The RGO dispersion (0.5 mg/ml) obtained was mixed with GO solution with different weight percent of RGO (RGO x wt% in GO, where $x = 0, 0.5, 1, 2, 5$) and sonicated and stirred overnight. For simplicity, RGO x wt% in GO matrix is here after referred to as RGO x%, where $x = 0, 0.5, 1, 2, 5$. The RGO/GO nano-hybrid dispersion was drop-cast on FTO and dried overnight to make FTO/RGO/GO nano-hybrid photoelectrode the photoelectrode was characterized and PEC water reduction activity was investigated.

Characterization

X-ray diffraction characterization was carried out on a D-2 phaser XRD300W diffractometer containing Cu K source. Field emission scanning electron microscopy (FESEM)

images were taken using JSM6500F, JEOL with an accelerating voltage of 15 kV. Diffuse reflectance UV–Visible spectra were acquired by JASCOV 560 UV–Vis spectrophotometer with $BaSO_4$ plate reference.

Photoelectrochemical measurement

The photoelectrochemical (PEC) characterization was measured using Ag–AgCl as reference electrode, Pt as counter electrode, and the RGO/GO nano-hybrid on FTO photoelectrode as the working electrode. HgXe (Newport, 500 W) light source fixed with AM1.5 G filter and calibrated to 100 mW/cm^2 (1 sun) was used. PEC characterization was done using 1 M H_2SO_4 electrolyte solution. An Autolab electrochemical work station with NOVA software was used for electrochemical measurement.

Result and discussion

The crystalline structure of the RGO/GO nano-hybrid was studied in comparison to GO and RGO. The XRD spectrum displayed in Fig. 1 presents peaks at 27°, 10.4°, 24°, and 12.2° for graphite, GO, RGO and RGO/GO nano-hybrid, respectively. These diffraction angles correspond to the inter-layer distance between graphitic sheets. The graphite diffraction peak centered at 27° corresponds to the lowest inter-layer distance between the graphite sheets and shifted to 10.4° after its oxidation to GO, showing the increased inter-layer spacing between the GO sheets as a result of introduction of oxygenated functionalities (–COC–, C=O, –OH, COOH) in the basal plane and on the edges.

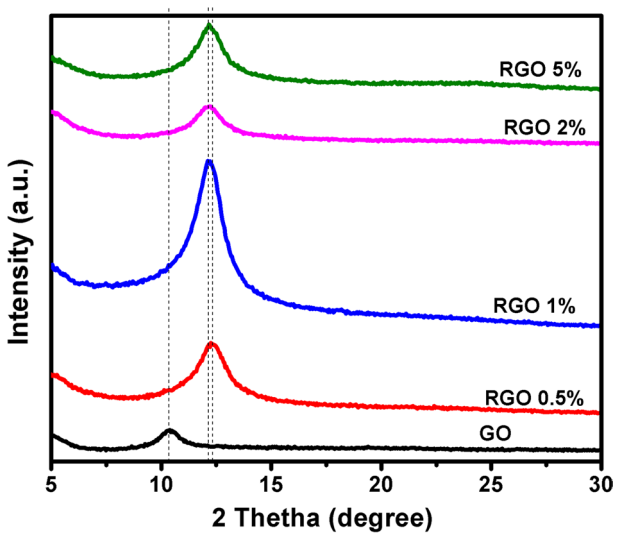

Fig. 1 XRD spectra of pristine GO and different weight percent RGO-incorporated RGO/GO nano-hybrid

Subsequent reduction removes most of the oxygenated functionalities from the surface of graphene oxide sheet, reducing the inter-layer spacing and hence upshifting the diffraction angle to 24°. The diffraction angles of the RGO/GO nano-hybrid (12.2°) lie between the values of GO and RGO. We can see that the amount of RGO in the hybrid is 0.5, 1, 2, and 5 wt% in the GO matrix. Regardless of its smaller amount, RGO causes a significant higher angle shift on the GO diffraction peak (a change of ~ 1.8°) implying that the addition of RGO influences the lattice structure of GO. In addition, the peak of RGO is absent in the RGO/GO, showing the absence of aggregated or stacked RGO sheets but fully utilized as nucleation site for GO to produce strongly coupled RGO/GO nano-hybrid. The higher angle shift in RGO/GO with respect to GO implies the decrease of inter-layer spacing as a result of strong coupling in RGO/GO. It could be due to a strong π–π stacking interaction between the electron-deficient GO and π-electron-rich RGO sheets. The increasing RGO loading amount from 0.5 to 5 wt% does not cause a significant change in the structure confirming that RGO sheets are acting as a nucleation center for growing a strongly coupled RGO/GO nano-hybrid. This is a result of strong π–π interactions between the graphitic planes of RGO and localized graphitic planes of GO. This strong interaction could have a positive effect on the charge transport properties of the composite material. In combining materials with conjugated π systems, it is reported that a stacked layer intercalation orientation is favorably formed by placing each conjugated π system in a parallel position over the plane of the other π system leading to strong π–π interactions [37]. Furthermore, XRD shows the absence of bulk phase separation between RGO and GO in the composite material.

The FTIR spectrum of GO, RGO, and RGO/GO nano-hybrid is presented in Fig. 2. In the case of GO, broad and intense peaks at about 3457 cm^{-1} are due to the stretching vibrations of –OH group from different alkoxy and carboxy functional groups [38]. The peaks at about 1720 and 1631 cm^{-1} are a result of C=O absorption from carboxylic species and C=C vibrations (O–H bending) from aromatic ring, respectively. The C–O–H vibration is also emerged at 1113 cm^{-1}. For RGO, the –OH vibrations peak is almost disappeared and an intense peak at 1557 cm^{-1} appeared, corresponding to the C=C stretching in the graphitic ring of RGO, confirming the formation of RGO. Moreover, the peak at 1203 cm^{-1} is due to the C–O–H vibrations. In RGO/GO nano-hybrid systems, the peak due to RGO is absent as a result of its smaller amount. The –OH vibration is notably reduced in height and redshifted. The red-shifting of the O–H band (weaker bond) in RGO/GO may indicate stronger hydrogen bonding and electrostatic interaction between trace amounts of epoxy(carbonyl) oxygen of RGO and hydroxyl units of GO [39, 40]. The C=O stretching vibration peak still existed in the RGO/GO hybrid with no significant shift.

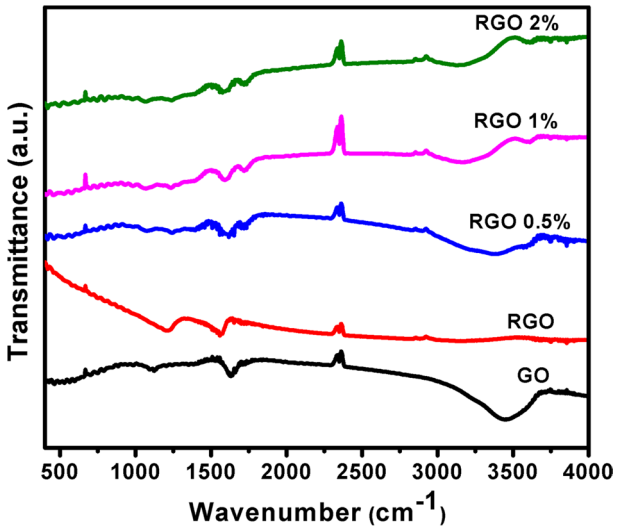

Fig. 2 FTIR spectra of pristine GO and RGO/GO nano-hybrid with various RGO weight percent

Whereas, O–H bending/C=C stretching vibration exhibited a reduced intensity and red-shift relative to GO for RGO/GO hybrid. In addition to the above-stated interactions, π–π stacking interactions between C=C in graphitic planes of RGO and localized benzenoid rings of GO play significant role for the red-shift [41–43]. The peak height of the OH bending and stretching vibrations are reduced for all compositions of RGO/GO hybrid which could be a result of lower water content due to lower hydrophilicity relative to GO. The FTIR analysis clearly indicates that the GO spectra are dominated by hydroxy, alkoxy, and epoxy groups, while the RGO is dominated by alkoxy and C=C bond. Therefore, we conclude that the coupling of GO and RGO was facilitated by hydrogen bond and π–π stacking interactions. The FTIR of the nano-hybrid illustrates the formation of a strongly coupled RGO/GO with an enhanced property suitable for optoelectronic applications.

UV–Vis absorption spectrum presented in Fig. 3a shows peak of GO dispersion at 296 nm. This is due to the n–π* transfer of the C=O bond in carbonyl and carboxyl functional groups [44, 45]. In addition, it also can arise from electronic transfer involving π and π* orbitals in the sp^2 clusters remained in the structure of GO after its oxidation [46]. After reduction, RGO exhibited increased and featureless absorption between 340 and 800 nm, typical absorbance of graphene suggesting the restoration of electronic conjugation [47]. RGO/GO displays more increased absorption compared with GO over wavelength range from 320 to 860 nm. This enhances the light collection efficiency of RGO/GO hybrid leading to better PEC efficiency. No significant difference in the absorption is seen with different weight percent of RGO in the RGO/GO hybrid, showing THAT only small quantity of RGO can change the structural, electrical and optical property of GO by rendering strong coupling between the sheets.

Figure 3b displays the corresponding Tauc plot, $(\alpha h\nu)^2$ with $h\nu$, of the GO and RGO/GO nano-hybrid, where h is the Planck constant and ν is the frequency. The energy gap E_g can be estimated by finding the x-intercept of an extrapolated Tauc plot. The band gap of GO is found to be about 3.11 eV and decreased to 2.58 eV for RGO/GO nano-hybrid. The lower energy gap for RGO/GO nano-hybrid leads to an

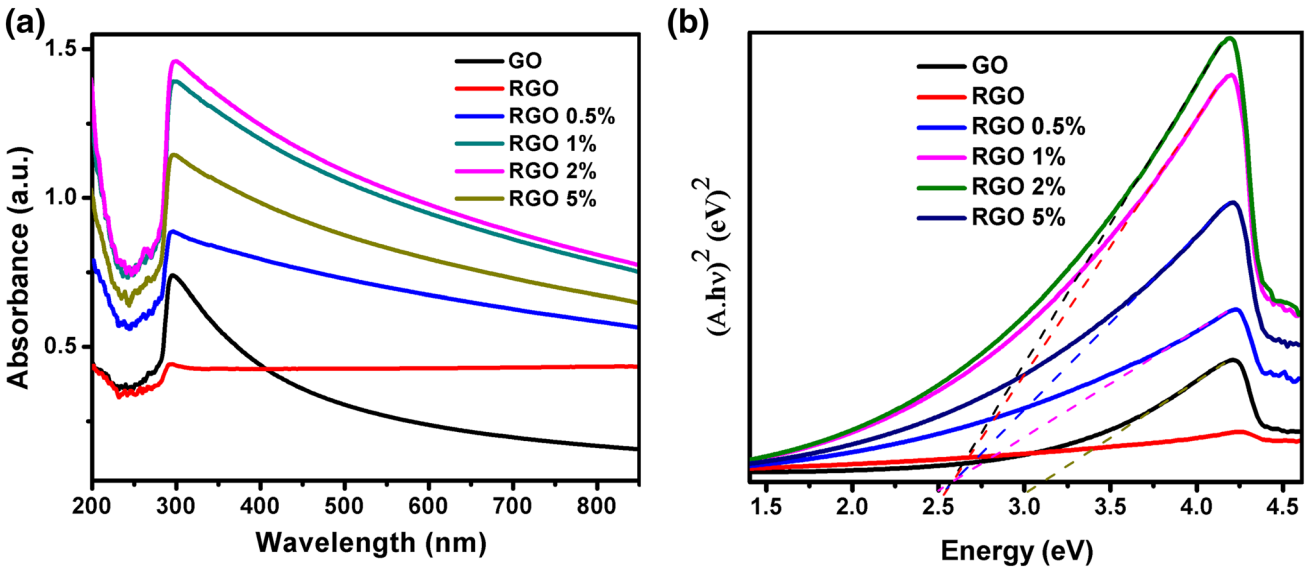

Fig. 3 UV–visible absorption spectra (**a**) and corresponding Tauc plots of pristine GO and RGO/GO nano-hybrid with various RGO weight percent (**b**)

extended absorption range to the visible region of the electromagnetic spectrum, which enhances the light harvesting efficiency of the RGO/GO.

The morphology of GO, RGO and the RGO/GO nano-hybrid is given in Fig. 4. A layered structure with some disorder is observed in each case, indicating their polycrystalline nature. Relatively, RGO/GO nano-hybrid exhibited more aggregation than GO. Incorporating small amount of RGO (e.g., 2 wt%) in the GO provides a seeding layer, leading to the formation of more compacted/stacked RGO/GO hybrid than GO. This is in agreement with the XRD, showing the lower d-spacing of RGO/GO. This could increase the electronic conductivity of GO, which in turn enhances the photoelectrode performance.

The C:O ratio of GO, RGO, and RGO/GO hybrid was examined using the EDS measurement (Fig. 5). The C:O ratio in GO, RGO and RGO/GO (5%) was 1.48, 6.76, and 2.53, respectively. As GO is the most oxidized form of graphite, its C:O is low due to high oxygen content; whereas in RGO, much of the oxygen content decreased and its C:O ratio is larger. In the RGO/GO, the C:O ratio is between the values of GO and RGO only. The EDS result confirms the conversion of GO to RGO. Due to the availability of a larger amount of oxygenated functionalities in GO, the ratio of C to O atoms is lower. After conversion of GO to RGO, the oxygenated functionalities were relatively removed, resulting in a higher amount of C–O ratio. The conversion process restores the graphitic planes in RGO sheet with traces of oxygenated functionalities leading to an enhancement in conductivity. This trace amount of oxygenated functionalities in RGO sheet could help it to interact with GO to build RGO/GO nano-hybrid.

The photoelectrochemical water reduction activities of pristine GO and different weight percent RGO (0.5, 1, 2, and 5 wt%)-incorporated GO nano-hybrid photoelectrode were studied in a three-electrode setup under chopped light illumination. A negligible current density (< -5 μA/cm^2) was measured under dark condition (light off) for all photoelectrodes and when the light is on, the photocurrent

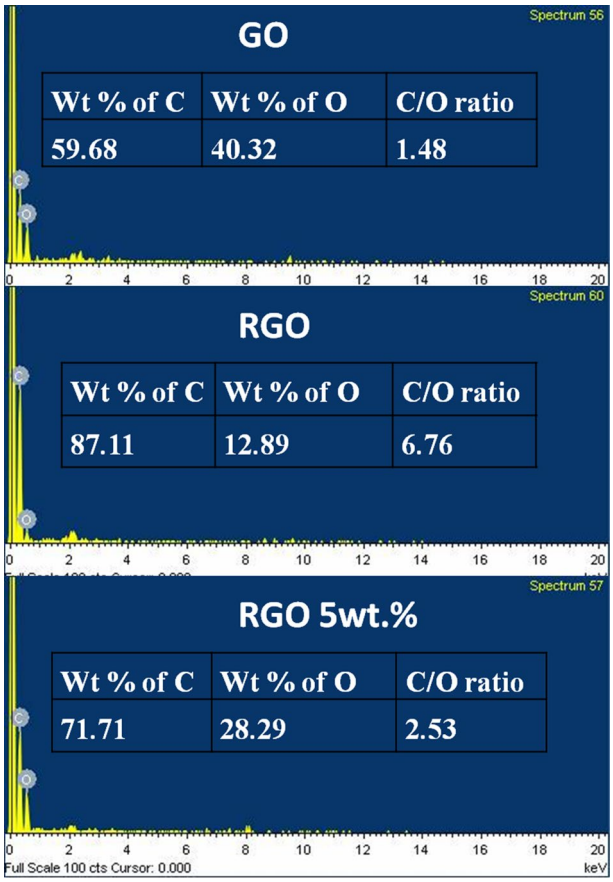

Fig. 5 EDS measurement of GO, RGO and RGO/GO hybrid (5%) and the corresponding C/O ratio

density jumped to a larger value. The amount of RGO in GO matrix was varied from 0.5 to 5 wt%. in the nano-hybrid and the resulting photocurrent density was -42.80, -45.20, -61.35, -48.99, -41.15 μA/cm^2 for pristine GO, RGO 0.5%, RGO 1%, RGO 2%, and RGO 5%, respectively, at a time of 60 s after light on during photoelectrolysis (Fig. 6a). Most of the nano-hybrids performed better than the pristine GO photoelectrode, where the maximum performance was

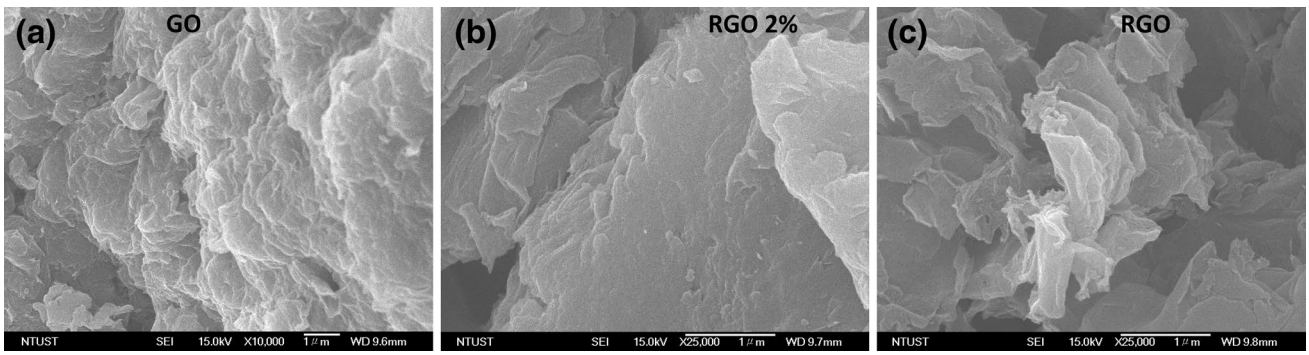

Fig. 4 SEM image of **a** GO, **b** RGO/GO nano-hybrid (2%) and **c** RGO. Scale bar 1 μm

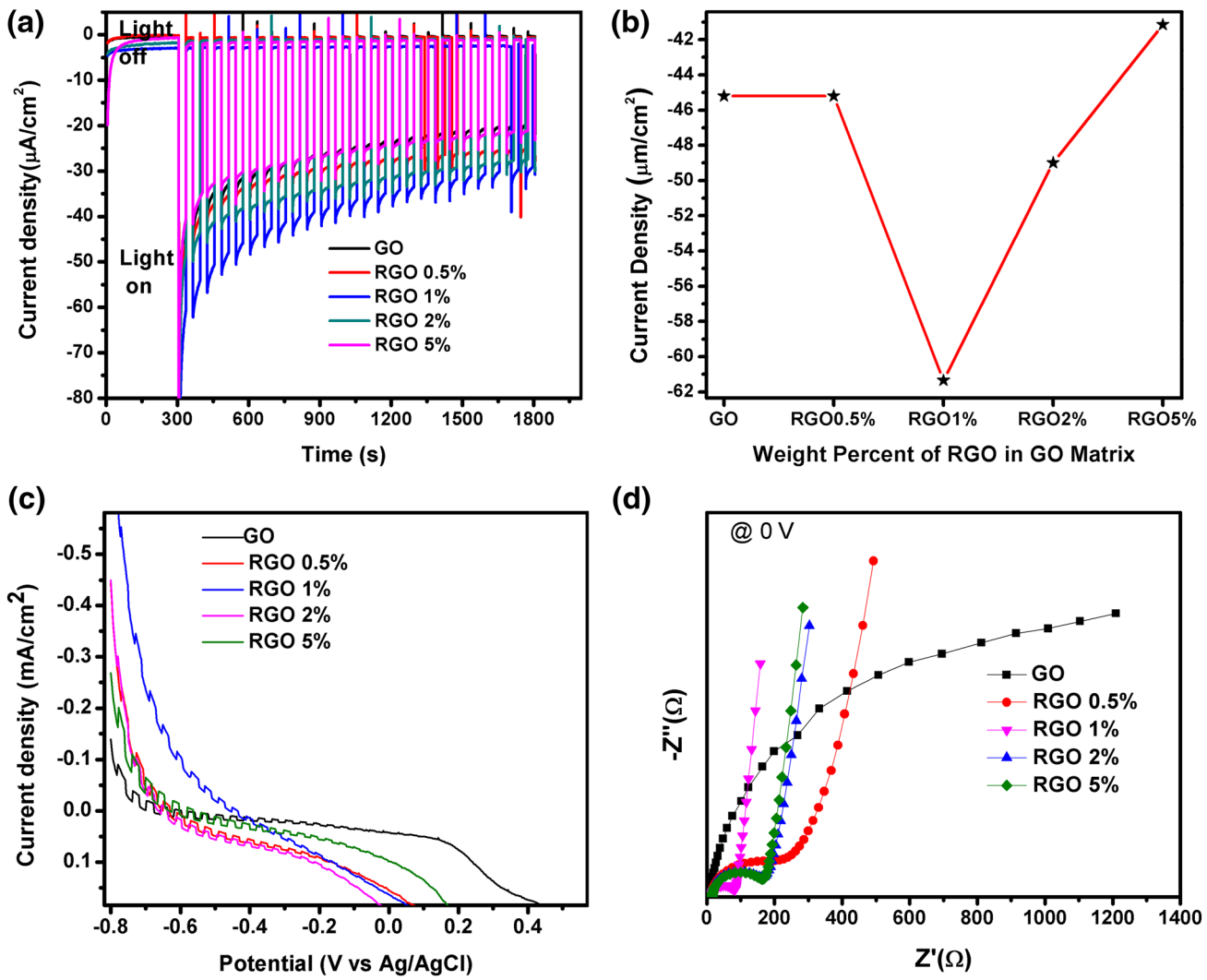

Fig. 6 **a** Photocurrent density–time profile obtained for GO and RGO (0.5, 1, 2, 5%)/GO nano-hybrid at 0 V vs. Ag/AgCl under chopped simulated sunlight. **b** Photocurrent density as a function of RGO wt% in GO after 60-s illumination. **c** Photocurrent density response versus applied for GO and RGO/GO hybrid photoelectrode under chopped simulated sunlight. **d** Electrochemical impedance spectroscopy measurement at 0 V vs Ag/AgCl. All measurements were performed in a three-electrode setup at a scan rate of 10 mV/s in 1 M H_2SO_4 aqueous solution. The light is calibrated to 1 sun simulated light (AM1.5 G, 100 mW/cm^2)

recorded for nano-hybrid composed of 1 wt% RGO in GO. The result shows improvement in performance of GO photoelectrode with increasing RGO amount from 0.5 to 1% and starts to decline when increasing its amount to 2 and 5%, with the maximum photocurrent density generated at 1% RGO (Fig. 6b). It is noted that RGO would promote charge carrier recombination if the concentration is too much [34]. This could be the reason for lower photocurrent generation for the higher percentage of RGO in GO nano-hybrid, signifying optimum RGO amount is 1% for best photocurrent conversion. Moreover, the stability of the nano-hybrid photoelectrode is also improved.

Figure 6c shows the resulting photocurrent from the *i–v* plot investigated in a PEC cell under a chopped simulated sunlight. The observed photocurrent is mainly cathodic indicating the RGO/GO nano-hybrid photoelectrode is predominantly p-type semiconductor. In addition, the flat band potential (Efb) of the GO and RGO/GO composites could be determined from the *i–v* plot using the onset potential methods [48]. The photocurrent changes sign at a potential greater than the flat band potential. Hence, the RGO 1% has more negative flat band potential compared to GO and other different compositions of RGO/GO nano-hybrid. This is one of the reasons why

RGO 1% has the best photocurrent compared to GO and other RGO/GO nano-hybrid. At more negative flat band potential, the nano-hybrid has sufficiently high potential to reduce water to hydrogen, and this reduction potential decreases with more positive flat band potential value of the photoelectrode.

The other mechanism of photocurrent enhancement for the RGO/GO nano-hybrid photoelectrode was investigated by electrochemical impedance spectroscopy measurement (Fig. 6d). The diameter of the semicircle in the impedance plot represents the charge transfer resistance between the photoelectrode and the solution. The smaller the diameter of the semicircle, the lower the charge transfer resistance of the materials (lower charge carrier recombination), and hence better charge conduction at the interface. GO exhibited the largest semicircle diameter, showing larger charge transfer resistance created at electrode–electrolyte interface. All RGO/GO electrodes resulted in lower semicircle diameter signifying the lower charge transfer resistance created at the electrode–electrolyte interface. Especially, the RGO 1% has lowest semicircle diameter indicating lowest charge transfer resistance of the electrode or lowest e–h recombination rate, and hence the best nano-hybrid photoelectrode with fast electron transfer kinetics for water reduction. This delivers maximum photoelectrochemical energy conversion.

The conduction band (CB) edge of GO and RGO/GO nano-hybrid was determined through the extrapolation of cathodic linear sweep voltammetry curves to the potential axis measured in dark condition as displayed in Fig. 7a [10, 12, 24]. The extrapolation crosses the potential axis at −0.52, −0.28, −0.60, −0.50, and −0.55 V vs Ag/AgCl for GO, RGO 0.5%/GO, RGO 1%/GO, RGO 2%/GO, and RGO 5%/GO, respectively. These potentials correspond to the conduction band CB edge. Hence, the nano-hybrid photoelectrode composed of RGO 1% in GO matrix possesses more negative CB edge relative to pristine GO and other RGO/GO hybrid photoelectrodes, which exhibited high photoconversion efficiency relative to other photoelectrodes. The result suggests that more negative photoelectrode potential leads to faster electron transfer rate, and hence lower carrier recombination rate, for hydrogen ion reduction. This is in agreement with the EIS result having lower diameter for the RGO 1%, indicating the lower charge transfer resistance. Here, RGO is used as a superior channel for electron collection and transportation. Recently, reports have shown this kind of property for RGO-incorporated composite [31, 49, 50]. In addition, RGO affects the band structure of the GO host as can be seen from the energy gap and conduction band edge values of pristine GO and RGO-incorporated GO. This is due to the strong π–π electronic interaction between GO and RGO sheets which is dependent on the concentration of RGO. The corresponding energy level diagram of GO and RGO (0.5, 1, 2, 5 wt%)/GO nano-hybrid with respect to water oxidation and reduction potentials is shown in Fig. 7b. From the energy level diagram, GO and all RGO/GO nano-hybrid possessed a conduction band edge more negative than the water reduction potential (− 0.197 V vs Ag/AgCl) and the valence band edge more positive than the water oxidation potential (1.03 V vs Ag/AgCl) in 1 M H_2SO_4 electrolyte solution. This shows the potential of the hybrid semiconductor material for overall water splitting purpose.

Figure 8 shows the schematic diagram of proposed photoelectron transport in GO and RGO/GO nano-hybrid photoelectrode during photoelectrochemical water reduction. Water reduction at the p-type GO-based photocathode produces hydrogen and the oxidation at the Pt counter electrode oxidizes water. The enhanced photocurrent generated in RGO/GO/FTO photoelectrode is due to the fast electron transport in the hybrid due to the superior electron collection and transportation property of RGO. The potential of the hybrid semiconductor material for overall water splitting purpose is encouraging. The method is feasible to apply for other layered semiconductor host materials and conjugated molecules which could create strong π–π interaction with RGO.

Conclusion

In summary, RGO-incorporated GO host was used to create RGO/GO nano-hybrid photoelectrode using a simple solution impregnation method. Due to a similar layered structure of GO and RGO, a strongly coupled RGO/GO structure was formed as a result of π–π stacking interaction between them. Moreover, the rich oxygenated functionalities of GO and rare oxygenated functionalities of RGO create hydrogen bonding and other noncovalent interactions between them as confirmed from FTIR analysis. As a result of this, an improved PEC performance was exhibited by the RGO/GO nano-hybrid compared to pristine GO. RGO exhibited faster electron acceptor and transporter role, in addition to affecting the electronic band structure of GO. The method is feasible to apply for other layered semiconductor host materials and conjugated molecules which could create π–π interaction with RGO. The research shows this could be a good way in improving the optoelectronic properties of layered semiconductor materials and conjugated molecules.

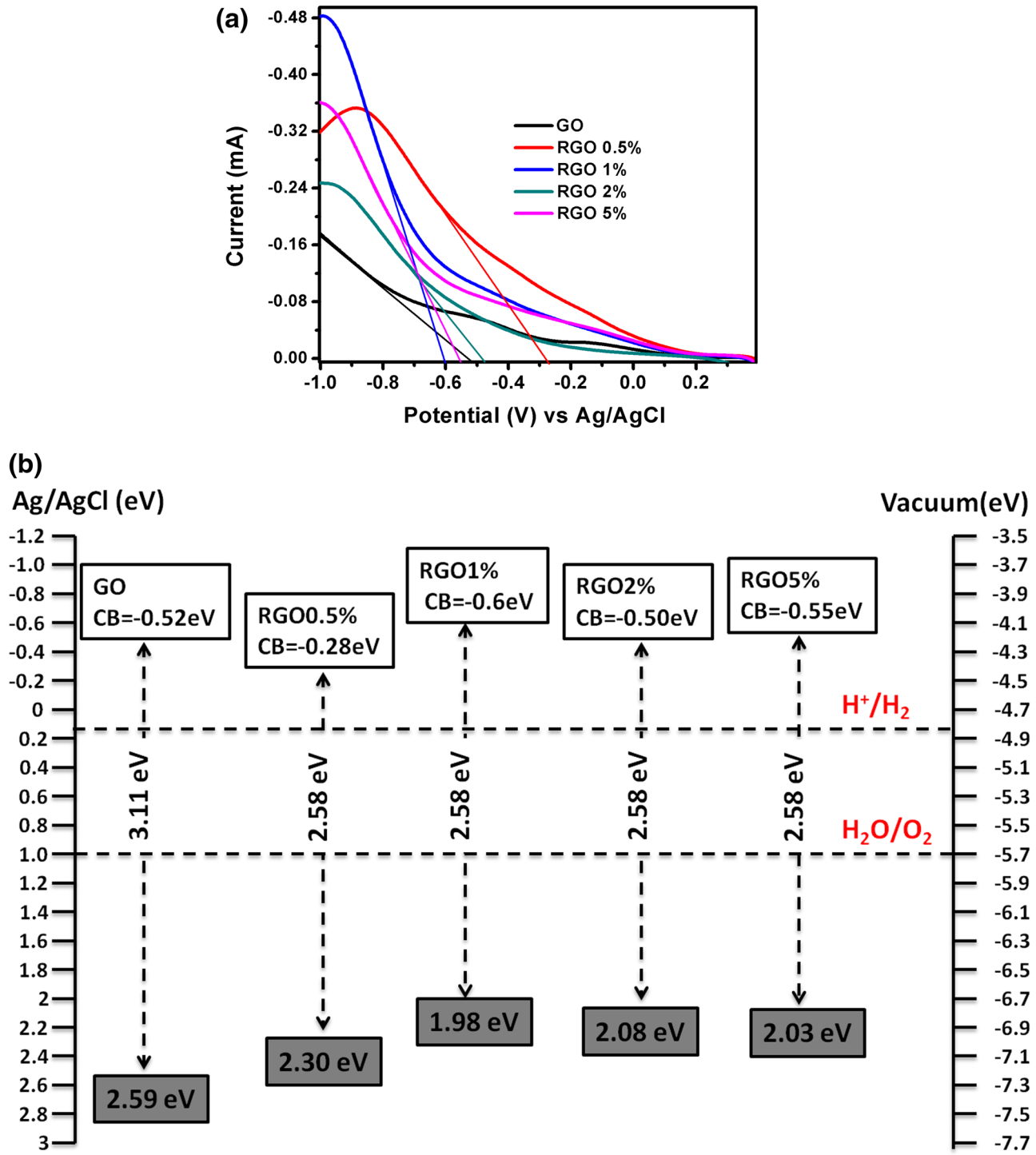

Fig. 7 **a** Cathodic linear sweep voltammetry in dark condition for determining the conduction band (CB) edge. All measurements were performed in a three-electrode setup at a scan rate of 10 mV/s in 1 M H_2SO_4 aqueous solution. **b** Schematic energy level diagram of GO and RGO (0.5, 1, 2, 5 wt%)/GO nano-hybrid with respect to water oxidation and reduction potentials

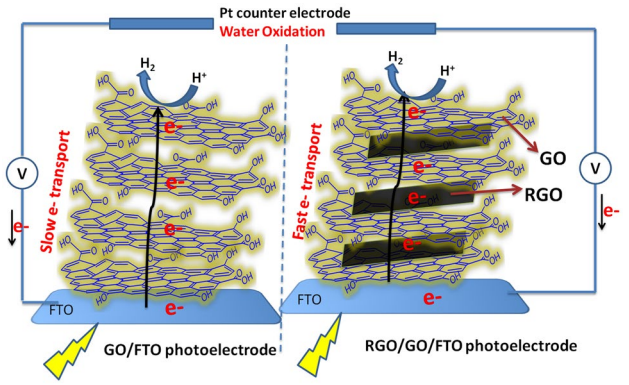

Fig. 8 Schematic diagram of proposed photoelectron transport in GO and RGO/GO nano-hybrid photoelectrode during photoelectrochemical water reduction

Acknowledgements NanoElectrochemistry Laboratory, Department of Chemical Engineering, National Taiwan University of Science and Technology (NTUST), Taiwan is acknowledged for SEM and EDS characterization.

References

1. Fujishima, A., Honda, K.: Electrochemical photolysis of water at a semiconductor electrode. Nature **238**, 37 (1972)
2. Aragaw, B.A., Pan, C.J., Su, W.N., Chen, H.M., Rick, J., Hwang, B.J.: Facile one-pot controlled synthesis of Sn and C codoped single crystal TiO_2 nanowire arrays for highly efficient photoelectrochemical water splitting. Appl. Catal. B Environ. **163**, 478–486 (2015)
3. Tamirat, A.G., Su, W.-N., Dubale, A.A., Chen, H.-M., Hwang, B.-J.: Photoelectrochemical water splitting at low applied potential using a NiOOH coated codoped (Sn, Zr) α-Fe_2O_3 photoanode. J. Mater. Chem. A **3**, 5949–5961 (2015)
4. Dubale, A.A., Pan, C.J., Tamirat, A.G., Chen, H.M., Su, W.N., Chen, C.H., Rick, J., Ayele, D.W., Aragaw, B.A., Lee, J.F., Yang, Y.W., Hwang, B.J.: Heterostructured Cu_2O/CuO decorated with nickel as a highly efficient photocathode for photoelectrochemical water reduction. J. Mater. Chem. A **3**, 12482–12499 (2015)
5. Dubale, A.A., Su, W.N., Tamirat, A.G., Pan, C.J., Aragaw, B.A., Chen, H.M., Chen, C.H., Hwang, B.J.: The synergetic effect of graphene on Cu_2O nanowire arrays as a highly efficient hydrogen evolution photocathode in water splitting. J. Mater. Chem. A **2**, 18383–18397 (2014)
6. Kalanur, S.S., Duy, L.T., Seo, H.: Recent progress in photoelectrochemical water splitting activity of WO_3 photoanodes. Top. Catal. **61**, 1043–1076 (2018)
7. Montes-Navajas, P., Asenjo, N.G., Santamaría, R., Menéndez, R., Corma, A., García, H.: Surface area measurement of graphene oxide in aqueous solutions. Langmuir **29**, 13443–13448 (2013)
8. Wang, X., Maeda, K., Thomas, A., Takanabe, K., Xin, G., Carlsson, J.M., Domen, K., Antonietti, M.: A metal-free polymeric photocatalyst for hydrogen production from water under visible light. Nat. Mater. **8**, 76 (2008)
9. Yeh, T.-F., Syu, J.-M., Cheng, C., Chang, T.-H., Teng, H.: Graphite oxide as a photocatalyst for hydrogen production from water. Adv. Funct. Mater. **20**, 2255–2262 (2010)
10. Yeh, T.-F., Chan, F.-F., Hsieh, C.-T., Teng, H.: Graphite oxide with different oxygenated levels for hydrogen and oxygen production from water under illumination: the band positions of graphite oxide. J. Phys. Chem. C **115**, 22587–22597 (2011)
11. Matsumoto, Y., Koinuma, M., Ida, S., Hayami, S., Taniguchi, T., Hatakeyama, K., Tateishi, H., Watanabe, Y., Amano, S.: Photoreaction of graphene oxide nanosheets in water. J. Phys. Chem. C **115**, 19280–19286 (2011)
12. Yeh, T.-F., Chen, S.-J., Yeh, C.-S., Teng, H.: Tuning the electronic structure of graphite oxide through ammonia treatment for photocatalytic generation of H_2 and O_2 from water splitting. J. Phys. Chem. C **117**, 6516–6524 (2013)
13. Mou, Z., Dong, Y., Li, S., Du, Y., Wang, X., Yang, P., Wang, S.: Eosin Y functionalized graphene for photocatalytic hydrogen production from water. Int. J. Hydrogen Energy **36**, 8885–8893 (2011)
14. Min, S., Lu, G.: Dye-sensitized reduced graphene oxide photocatalysts for highly efficient visible-light-driven water reduction. J. Phys. Chem. C **115**, 13938–13945 (2011)
15. Yeh, T.-F., Cihlář, J., Chang, C.-Y., Cheng, C., Teng, H.: Roles of graphene oxide in photocatalytic water splitting. Mater. Today **16**, 78–84 (2013)
16. Chen, D., Zhang, H., Liu, Y., Li, J.: Graphene and its derivatives for the development of solar cells, photoelectrochemical, and photocatalytic applications. Energy Environ. Sci. **6**, 1362–1387 (2013)
17. Krishnamoorthy, K., Mohan, R., Kim, S.J.: Graphene oxide as a photocatalytic material. Appl. Phys. Lett. **98**, 244101 (2011)
18. Oh, J., Chang, Y.H., Kim, Y.-H., Park, S.: Thickness-dependent photocatalytic performance of graphite oxide for degrading organic pollutants under visible light. PCCP **18**, 10882–10886 (2016)
19. Hsu, H.-C., Shown, I., Wei, H.-Y., Chang, Y.-C., Du, H.-Y., Lin, Y.-G., Tseng, C.-A., Wang, C.-H., Chen, L.-C., Lin, Y.-C., Chen, K.-H.: Graphene oxide as a promising photocatalyst for CO_2 to methanol conversion. Nanoscale **5**, 262–268 (2013)
20. Kumar, P., Bansiwal, A., Labhsetwar, N., Jain, S.L.: Visible light assisted photocatalytic reduction of CO_2 using a graphene oxide supported heteroleptic ruthenium complex. Green Chem. **17**, 1605–1609 (2015)
21. Marszewski, M., Cao, S., Yu, J., Jaroniec, M.: Semiconductor-based photocatalytic CO_2 conversion. Mater. Horiz. **2**, 261–278 (2015)
22. Kumar, S., Yadav, R.K., Ram, K., Aguiar, A., Koh, J., Sobral, A.J.F.N.: Graphene oxide modified cobalt metallated porphyrin photocatalyst for conversion of formic acid from carbon dioxide. J. CO2 Util. **27**, 107–114 (2018)
23. Kumar, S., Wani, M.Y., Arranja, C.T., Castro, R.A.E., Paixão, J.A., Sobral, A.J.F.N.: Synthesis, physicochemical and optical properties of bis-thiosemicarbazone functionalized graphene oxide. Spectrochim. Acta A **188**, 183–188 (2018)
24. Sun, L., Du, T., Hu, C., Chen, J., Lu, J., Lu, Z., Han, H.: Antibacterial activity of graphene oxide/g-C_3N_4 composite through

photocatalytic disinfection under visible light. ACS Sustain. Chem. Eng. **5**, 8693–8701 (2017)
25. Liu, Y., Zeng, X., Hu, X., Hu, J., Zhang, X.: Two-dimensional nanomaterials for photocatalytic water disinfection: recent progress and future challenges. J. Chem. Technol. Biotechnol. **94**, 22–37 (2019)
26. Wei, Y., Zhu, Y., Jiang, Y.: Photocatalytic self-cleaning carbon nitride nanotube intercalated reduced graphene oxide membranes for enhanced water purification. Chem. Eng. J. **356**, 915–925 (2019)
27. Ng, Y.H., Iwase, A., Kudo, A., Amal, R.: Reducing graphene oxide on a visible-light $BiVO_4$ photocatalyst for an enhanced photoelectrochemical water splitting. J. Phys. Chem. Lett. **1**, 2607–2612 (2010)
28. Wang, H., Dai, H.: Strongly coupled inorganic–nano-carbon hybrid materials for energy storage. Chem. Soc. Rev. **42**, 3088–3113 (2013)
29. Wang, N., Zhou, Y., Chen, C., Cheng, L., Ding, H.: A g-C_3N_4 supported graphene oxide/Ag_3PO_4 composite with remarkably enhanced photocatalytic activity under visible light. Catal. Commun. **73**, 74–79 (2016)
30. Tamirat, A.G., Su, W.-N., Dubale, A.A., Pan, C.-J., Chen, H.-M., Ayele, D.W., Lee, J.-F., Hwang, B.-J.: Efficient photoelectrochemical water splitting using three dimensional urchin-like hematite nanostructure modified with reduced graphene oxide. J. Power Sources **287**, 119–128 (2015)
31. Ng, Y.H., Lightcap, I.V., Goodwin, K., Matsumura, M., Kamat, P.V.: To what extent do graphene scaffolds improve the photovoltaic and photocatalytic response of TiO_2 nanostructured films? J. Phys. Chem. Lett. **1**, 2222–2227 (2010)
32. Xiang, Q., Yu, J., Jaroniec, M.: Preparation and enhanced visible-light photocatalytic H_2-production activity of graphene/C_3N_4 composites. J. Phys. Chem. C **115**, 7355–7363 (2011)
33. Babu, S.G., Vinoth, R., Narayana, P.S., Bahnemann, D., Neppolian, B.: Reduced graphene oxide wrapped Cu_2O supported on C_3N_4: an efficient visible light responsive semiconductor photocatalyst. APL Mater. **3**, 104415 (2015)
34. Zhang, Y., Mori, T., Niu, L., Ye, J.: Non-covalent doping of graphitic carbon nitride polymer with graphene: controlled electronic structure and enhanced optoelectronic conversion. Energy Environ. Sci. **4**, 4517–4521 (2011)
35. Hunter, C.A., Sanders, J.K.M.: The nature of π–π interactions. J. Am. Chem. Soc. **112**, 5525–5534 (1990)
36. Hummers, W.S., Offeman, R.E.: Preparation of graphitic oxide. J. Am. Chem. Soc. **80**, 1339 (1958)
37. Umadevi, D., Panigrahi, S., Sastry, G.N.: Noncovalent Interaction of Carbon Nanostructures. Acc. Chem. Res. **47**, 2574–2581 (2014)
38. Coates, J.P.: The interpretation of infrared spectra: published reference sources. Appl. Spectrosc. Rev. **31**, 179–192 (1996)
39. Gao, W.: The chemistry of graphene oxide. In: Gao, W. (ed.) Graphene oxide: reduction recipes, spectroscopy, and applications, pp. 61–95. Springer International Publishing, Cham (2015)
40. Dreyer, D.R., Park, S., Bielawski, C.W., Ruoff, R.S.: The chemistry of graphene oxide. Chem. Soc. Rev. **39**, 228–240 (2010)
41. Wang, H., Hao, Q., Yang, X., Lu, L., Wang, X.: Graphene oxide doped polyaniline for supercapacitors. Electrochem. Commun. **11**, 1158–1161 (2009)
42. Georgakilas, V., Tiwari, J.N., Kemp, K.C., Perman, J.A., Bourlinos, A.B., Kim, K.S., Zboril, R.: Noncovalent functionalization of graphene and graphene oxide for energy materials, biosensing, catalytic, and biomedical applications. Chem. Rev. **116**, 5464–5519 (2016)
43. Sun, Y., Li, C., Xu, Y., Bai, H., Yao, Z., Shi, G.: Chemically converted graphene as substrate for immobilizing and enhancing the activity of a polymeric catalyst. Chem. Commun. **46**, 4740–4742 (2010)
44. Rabchinskii, M.K., Dideikin, A.T., Kirilenko, D.A., Baidakova, M.V., Shnitov, V.V., Roth, F., Konyakhin, S.V., Besedina, N.A., Pavlov, S.I., Kuricyn, R.A., Lebedeva, N.M., Brunkov, P.N., Vul', A.Y.: Facile reduction of graphene oxide suspensions and films using glass wafers. Sci. Rep. **8**, 14154 (2018)
45. Kumar, P.V., Bardhan, N.M., Tongay, S., Wu, J., Belcher, A.M., Grossman, J.C.: Scalable enhancement of graphene oxide properties by thermally driven phase transformation. Nat. Chem. **6**, 151 (2013)
46. Yan, J.-A., Xian, L., Chou, M.Y.: Structural and electronic properties of oxidized graphene. Phys. Rev. Lett. **103**, 086802 (2009)
47. Li, D., Müller, M.B., Gilje, S., Kaner, R.B., Wallace, G.G.: Processable aqueous dispersions of graphene nanosheets. Nat. Nanotechnol. **3**, 101 (2008)
48. Beranek, R.: (Photo)electrochemical methods for the determination of the band edge positions of TiO_2-based nanomaterials. Adv. Phys. Chem. **2011**, 20 (2011)
49. Liu, Z., Liu, Q., Huang, Y., Ma, Y., Yin, S., Zhang, X., Sun, W., Chen, Y.: Organic photovoltaic devices based on a novel acceptor material: graphene. Adv. Mater. **20**, 3924–3930 (2008)
50. Tang, Y.-B., Lee, C.-S., Xu, J., Liu, Z.-T., Chen, Z.-H., He, Z., Cao, Y.-L., Yuan, G., Song, H., Chen, L., Luo, L., Cheng, H.-M., Zhang, W.-J., Bello, I., Lee, S.-T.: Incorporation of graphenes in nanostructured TiO_2 films via molecular grafting for dye-sensitized solar cell application. ACS Nano **4**, 3482–3488 (2010)